Raman Spectroscopy and Microwave Dielectric Properties of $Zr_{1-x}(Li_{1/4}Nb_{3/4})_xTiO_4$ Ceramics

Li-Xia Pang, Hong Wang*, Di Zhou, and Xi Yao

Electronic Materials Research Laboratory, Key Laboratory of the Ministry of Education, Xi'an Jiaotong University, Xi'an 710049, China

Received November 19, 2008; accepted January 28, 2009; published online May 20, 2009

The phase evolution, sintering behavior, and microwave dielectric properties of the $Zr_{1-x}(Li_{1/4}Nb_{3/4})_xTiO_4$ system were investigated. The phase evolution of $Zr_{1-x}(Li_{1/4}Nb_{3/4})_xTiO_4$ was studied by X-ray diffraction analysis, scanning electron microscopy, and Raman spectroscopy. Raman analysis showed that the chemical substitution of $(Li_{1/4}Nb_{3/4})$ for Zr in the $ZrTiO_4$ system enhanced the kinetics of ordering reactions to form the $Z^{TT}Z_{TT}$ sequence (crystallized as the $Zr_5Ti_7O_{24}$ phase). The abnormal Raman band centered at 868–878 cm^{-1} in the $Zr_{1-x}(Li_{1/4}Nb_{3/4})_xTiO_4$ ceramics may indicate the short-range cation ordering of Li/Nb. Without any sintering aids, the sintering temperature of the $Zr_{1-x}(Li_{1/4}Nb_{3/4})_xTiO_4$ ceramics was lowered to 1110–1200 °C, which was much lower than that of $ZrTiO_4$ (higher than 1400 °C). The dielectric constant (ε_r) of the $Zr_{1-x}(Li_{1/4}Nb_{3/4})_xTiO_4$ ceramic increased from 34.5 to 46.6 and the temperature coefficient of resonant frequency (TCF) shifted from −1.2 to +75 ppm/°C as the content of $(Li_{1/4}Nb_{3/4})$ substitution increased from 0.3 to 0.5. The phase evolution of $Zr_{1-x}(Li_{1/4}Nb_{3/4})_xTiO_4$ was responsible for the variation in its dielectric properties.

DOI: 10.1143/JJAP.48.051403

1. Introduction

In recent years, $ZrTiO_4$ (ZT) ceramics have attracted much interest owing to their specific electrical and structural properties,[1] and zirconium titanate-based ceramics have been developed for electronic applications, such as resonator components in filters and frequency-stable oscillators at microwave frequencies, where low-loss and temperature-stable dielectric materials are required.

In the ZrO_2–TiO_2 system near the composition $ZrTiO_4$, two structural modifications are known: a high-temperature disordered $Zr_{1+x}Ti_{1-x}O_4$ $(-1/6 < x < 1/10)$ phase and a low-temperature ordered $ZrTiO_4$ phase.[2–6] The high-temperature disordered phase crystallizes in the orthorhombic α-PbO_2 structure with space group *Pbcn*. Zr and Ti randomly distribute in the octahedral site at atmospheric pressure when the temperature exceeds 1400 °C and persist metastably at lower temperatures because the ordering process is sluggish. In the ZrO_2–TiO_2 system, there are two types of ordered structure with different stoichiometries both stable below 1200 °C:[2,5]

i) The stacking of two layers of distorted Zr sites and two layers of octahedral Ti sites alternately along the *a*-axis gives rise to a doubling of the cell parameter *a*; this ordering scheme is consistent with the formula $ZrTiO_4$ (low-*T* ordered $ZrTiO_4$).

ii) Zr is hosted in one of every three cation layers (Zr site approaches eightfold coordination) so that the cell parameter *a* is threefold, as is consistent with the mineral srilankite AB_2O_6 structure. In this case the formula is close to $ZrTi_2O_6$ but the same structure also occurs in $Zr_5Ti_7O_{24}$.[5]

With the extensive use of $ZrTiO_4$, the interest in its preparation, crystalline structure, microstructure, phase transformations, and property enhancement by chemical additives has increased. Marked progress has been made in understanding the effects of these factors on dielectric and sensing properties.[7,8] There have been several reports on the effects of chemical substitutions on the structures and properties of zirconium titanates.[1,5,9] A small uncoupled substitution of Y for Zr enhances the kinetics of the ordering reactions[5] but Hf and Sn substitutions are clearly effective in suppressing the driving force for long-range cation-ordering reactions.[9] Moreover, Sn substitution for Zr improved the densification behavior in the $ZrTiO_4$ system. $ZrTiO_4$ with 20 mol % Zr replaced by Sn ions showed excellent microwave dielectric properties with a dielectric constant ε_r of 38, a quality factor Q of 8000 at 7 GHz, and a temperature coefficient of resonant frequency TCF of 0 ppm/°C,[10–12] which was proved to be one of the best dielectric resonator materials for microwave devices. However, the sintering temperature of $Zr_xSn_yTi_zO_4$ $(x + y + z = 2)$ is still very high (above 1400 °C) and it is very difficult to lower the sintering temperature without marked deterioration in the microwave dielectric properties.

In this work, $(Li_{1/4}Nb_{3/4})$ was selected to substitute Zr in the $ZrTiO_4$ system because the equivalent ionic radius of $(Li_{1/4}Nb_{3/4})$ (0.67 Å, CN = 6) is similar to that of Zr (0.72 Å, CN = 6) (where CN is the coordination number).[13] On the other hand, $(Li_{1/4}Nb_{3/4})$ substitution for Ti in the rutile TiO_2 system effectively lowered the sintering temperature of TiO_2 ceramics from 1400 to 990 °C.[14] $Zr_{1-x}(Li_{1/4}Nb_{3/4})_xTiO_4$ $(0 \le x \le 0.5)$ ceramics are prepared by the conventional solid state reaction method in this work. The structural and microstructural changes across the solid solutions are characterized by X-ray diffraction (XRD) analysis, and scanning electron microscopy (SEM). For $Zr_{1-x}(Li_{1/4}Nb_{3/4})_xTiO_4$ $(0 \le x \le 0.5)$ ceramics crystallized at low sintering temperatures, cation ordering is not negligible microstructural information. In this work, Raman spectroscopy is used to determine whether cation ordering occurred in the $Zr_{1-x}(Li_{1/4}Nb_{3/4})_xTiO_4$ $(0 \le x \le 0.5)$ ceramics and which type of cation ordering it is. These data are then used to investigate the phase evolution and interpret the microwave dielectric properties in the $Zr_{1-x}(Li_{1/4}Nb_{3/4})_xTiO_4$ system.

2. Experimental Procedure

The compositions of $Zr_{1-x}(Li_{1/4}Nb_{3/4})_xTiO_4$ $(0 \le x \le 0.5)$ and $Zr_5Ti_7O_{24}$ were prepared by the conventional solid state

*E-mail address: hwang@mail.xjtu.edu.cn

reaction method using high-purity reagent-grade raw materials of Li_2CO_3 (>99% Guo-Yao), Nb_2O_5 (>99% Zhu-Zhou Harden Alloys.), rutile TiO_2 (>99% Linghua.), and ZrO_2 (>99.5% Xinxing). The raw materials were weighted according to the compositions of $Zr_{1-x}(Li_{1/4}Nb_{3/4})_xTiO_4$ ($0 \le x \le 0.5$) and $Zr_5Ti_7O_{24}$, and ball milled for 4.5 h using a planetary mill (Nanjing Machine Factory) with zirconia balls (2 mm in diameter) as the milling media. The mixtures were calcined at 950–1100 °C for 5 h and then remilled for 5 h using zirconia balls in deionized water. The milled powders were dried and granulated with a poly(vinyl alcohol) (PVA) binder and pressed into cylinders (10 mm in diameter and 5 mm in height) in a steel die under a uniaxial pressure of 20 kN/cm^2. The cylinders were sintered in air at 1080–1500 °C for 3 h.

The crystalline phases of the samples were investigated by X-ray diffractometry (XRD) with Cu Kα radiation (Rigaku D/MAX-2400). The apparent densities were measured by Archimedes' method. The microstructures of the fracture surfaces of the $Zr_{1-x}(Li_{1/4}Nb_{3/4})_xTiO_4$ ($0.3 \le x \le 0.5$) ceramics were observed by scanning electron microscopy (SEM; JEOL JSM-6360LV). Raman spectra ranging from 100 to 1000 cm^{-1} of the powders of the $Zr_{1-x}(Li_{1/4}Nb_{3/4})_xTiO_4$ ($0 \le x \le 0.5$) and $Zr_5Ti_7O_{24}$ ceramics were obtained using a Raman spectrometer (Nicolet ALMEGA), equipped with a diffraction grating of 2400 lines/mm, a spectrograph aperture with a 25 μm slit. The microscope attachment was an Olympus BX50 system and the excitation wavelength used was 532 nm from a Nd:YVO_4 laser source. The dielectric behaviors of the samples at microwave frequencies were measured by the $TE_{01\delta}$ shielded cavity method using a network analyzer (Agilent 8720ES) and a temperature chamber (Delta Design DELTA 9023). TCF was calculated using the following formula:

$$\mathrm{TCF} = \frac{f_{85} - f_{25}}{f_{25}(85 - 25)}, \qquad (1)$$

where f_{85} and f_{25} are the $TE_{01\delta}$ resonant frequencies at 85 and 25 °C, respectively.

3. Results and Discussion

Figure 1 shows the relative densities of the $Zr_{1-x}(Li_{1/4}Nb_{3/4})_xTiO_4$ ($0.3 \le x \le 0.5$) ceramics as a function of sintering temperature. As observed, the relative densities of the $Zr_{1-x}(Li_{1/4}Nb_{3/4})_xTiO_4$ ($0.3 \le x \le 0.5$) ceramics reached over 96% at 1140 °C, which indicated that the sintering temperature of the $ZrTiO_4$ ceramics was effectively lowered from 1500 to 1140 °C by the substitution of $(Li_{1/4}Nb_{3/4})$ for Zr. It was also observed in Fig. 1 that the relative density of the $Zr_{0.7}(Li_{1/4}Nb_{3/4})_{0.3}TiO_4$ ($x = 0.3$) ceramic was slightly lower than those of the $Zr_{0.6}(Li_{1/4}Nb_{3/4})_{0.4}TiO_4$ and $Zr_{0.5}(Li_{1/4}Nb_{3/4})_{0.5}TiO_4$ ($x = 0.4, 0.5$) ceramics. Figure 2 shows the typical backscattered electron images (BEIs) of the fracture surfaces of the $Zr_{1-x}(Li_{1/4}Nb_{3/4})_xTiO_4$ ($x = 0.3, 0.4, 0.5$) ceramics sintered at 1140 °C. The $Zr_{1-x}(Li_{1/4}Nb_{3/4})_xTiO_4$ ($x = 0.4, 0.5$) ceramics showed dense microstructures with nearly no pores while there were still a few in the $Zr_{0.7}(Li_{1/4}Nb_{3/4})_{0.3}TiO_4$ ($x = 0.3$) ceramic matrix. This is why the $Zr_{0.7}(Li_{1/4}Nb_{3/4})_{0.3}TiO_4$ ($x = 0.3$) ceramic showed a lower relative density than the others (as shown in Fig. 1). The grain sizes of the $Zr_{0.7}(Li_{1/4}Nb_{3/4})_{0.3}TiO_4$ ($x = 0.3$) ceramic and the $Zr_{0.6}(Li_{1/4}Nb_{3/4})_{0.4}TiO_4$ ($x = 0.4$) ceramic sintered at 1140 °C were between 1–4 and 2–3 μm, respectively, and it increased to 2.5–5 μm in the $Zr_{1-x}(Li_{1/4}Nb_{3/4})_xTiO_4$ ($x = 0.5$) ceramic sintered at the same sintering temperature. Thus, the relative density of the $Zr_{1-x}(Li_{1/4}Nb_{3/4})_xTiO_4$ ceramic still increased slightly when the content of $(Li_{1/4}Nb_{3/4})$ substitution increased from 0.4 to 0.5. Li_2O is effective for lowering the sintering temperature of titanate-based ceramics because structural vacancies are generated during its reaction with the matrix phase during the sintering process and sintering rate increases.[15] The mechanism of low-temperature sintering in the $Zr_{1-x}(Li_{1/4}Nb_{3/4})_xTiO_4$ system may be similar to that in the Li_2O-doped $SrTiO_3$ system.[15]

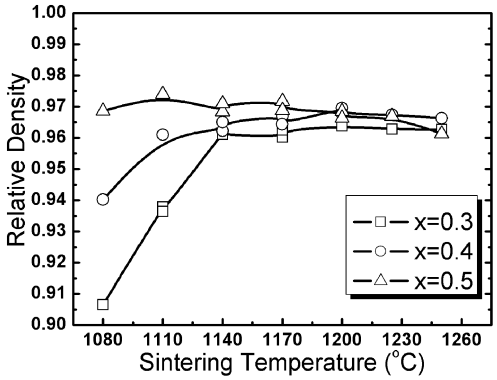

Fig. 1. Relative densities of $Zr_{1-x}(Li_{1/4}Nb_{3/4})_xTiO_4$ ($0.3 \le x \le 0.5$) ceramics as a function of sintering temperature.

In this study, BEIs and XRD patterns of the samples were used to study the phase evolution of the $(Li_{1/4}Nb_{3/4})$-substituted $ZrTiO_4$ system. The BEIs of the fracture surfaces of the $Zr_{1-x}(Li_{1/4}Nb_{3/4})_xTiO_4$ ($0.3 \le x \le 0.5$) ceramics in Fig. 2 showed that the color of all the grains was uniform in each ceramic matrix, which suggests that no secondary phase grains were detected. Figure 3 shows the XRD patterns of the sintered $Zr_{1-x}(Li_{1/4}Nb_{3/4})_xTiO_4$ ($x = 0, 0.3, 0.4, 0.5$) series and the $Zr_5Ti_7O_{24}$ ceramic. In the ZrO_2–TiO_2 system, the phase of compositions close to 5 : 7 was a commensurate ordered structure with a tripled a-axis superstructure and a $Z^{TT}Z_{TT}$ sequence.[16] By comparing the XRD pattern of the $Zr_5Ti_7O_{24}$ ceramic with that of the $ZrTiO_4$ ceramic in Fig. 3, it was observed that the diffraction peaks at $2\theta = 27.2°$ (211) and 53.6° appeared in the XRD pattern of the $Zr_5Ti_7O_{24}$ ceramic. As shown in Fig. 3, the diffraction peaks of $Zr_{1-x}(Li_{1/4}Nb_{3/4})_xTiO_4$ ($x = 0.3, 0.4, 0.5$) could be indexed as the $Zr_5Ti_7O_{24}$ phase, and the diffraction peak of (600) dispersed from that of (021) as the content of $(Li_{1/4}Nb_{3/4})$ substitution increased. On the other hand, the intensities of the diffraction peaks at $2\theta = 27.2$ and 53.6° increased with x value. This indicates that the substitution of $(Li_{1/4}Nb_{3/4})$ for Zr in $ZrTiO_4$ enhanced the kinetics of ordering reactions to form the $Z^{TT}Z_{TT}$ sequence.

The high-temperature cation-disordered $ZrTiO_4$ is represented by an α-PbO_2 structure with the space group *Pbcn* and the point group *mmm*. The normal vibration modes, obtained by applying the group factor analysis, predict that the high-temperature $ZrTiO_4$ phase (considering zirconium and titanium ions as one type of averaged ion) has 18 distinct Raman-active optical phonon modes.[17,18] The representation

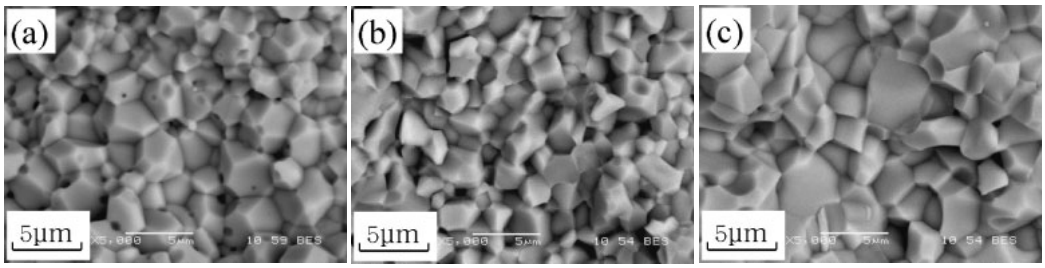

Fig. 2. BEIs of fracture surfaces of $Zr_{1-x}(Li_{1/4}Nb_{3/4})_xTiO_4$ ceramics sintered at 1140 °C: (a) $x = 0.3$; (b) $x = 0.4$; (c) $x = 0.5$.

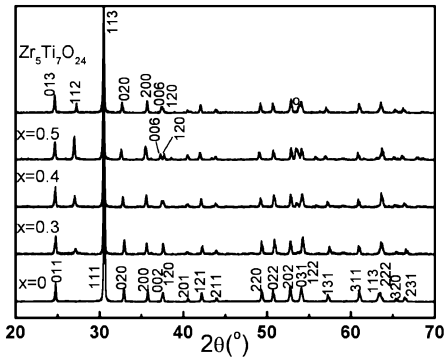

Fig. 3. XRD patterns of powders of $Zr_{1-x}(Li_{1/4}Nb_{3/4})_xTiO_4$ ceramics: $x = 0$ sintered at 1450 °C; $x = 0.3$, 0.4, 0.5 sintered at 1200 °C, and $Zr_5Ti_7O_{24}$ sintered at 1450 °C.

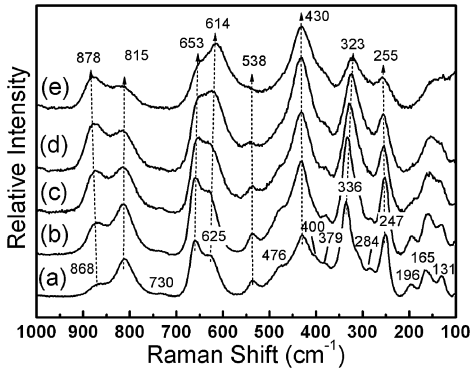

Fig. 4. Raman spectra of Zr_{1-x} $(Li_{1/4}Nb_{3/4})_xTiO_4$ ceramics: (a) $x = 0.1$ sintered at 1400 °C; (b) $x = 0.2$ sintered at 1400 °C; (c) $x = 0.3$ sintered at 1200 °C; (d) $x = 0.4$ sintered at 1200 °C; (e) $x = 0.5$ sintered at 1200 °C.

of the Raman active normal modes (Γ_{RA}) can be written using the following nondegenerate irreducible representation:

$$\Gamma_{RA} = 4A_g + 5B_{1g} + 4B_{2g} + 5B_{3g}. \quad (2)$$

The group factor analysis of the $Zr_5Ti_7O_{24}$ structure can be based on the structural model of the space group *Pbcn* ($Z = 4$) with the statistical occupation of A sites [symmetry 4c (2)] by 0.968 Zr and 0.032 Ti ions and B sites [symmetry 8d (1)] by 0.889 Ti and 0.111 Zr ions. The oxygen atoms are in general 8d (1) sites.[19] Considering that the A and B sites were occupied by the mixture of zirconium and titanium ions, accordingly, the Raman active normal modes (Γ_{RA}) of the $Zr_5Ti_7O_{24}$ structure can be written as the following nondegenerate irreducible representation:[17]

$$\Gamma_{RA} = 13A_g + 14B_{1g} + 13B_{2g} + 14B_{3g}. \quad (3)$$

The above group factor analysis predicts that $Zr_5Ti_7O_{24}$ has 54 distinct Raman-active optical phonon modes.

Figure 4 shows the room-temperature Raman spectra of the $Zr_{1-x}(Li_{1/4}Nb_{3/4})_xTiO_4$ ($0.1 \le x \le 0.5$) ceramics in the frequency range of 100–1000 cm^{-1} and Table I presents the locations of the Raman bands of the $Zr_5Ti_7O_{24}$[17] and $ZrTiO_4$ ceramic cooled at 1 °C/h,[17] air-quenched $ZrTiO_4$,[18] and the Zr_{1-x} $(Li_{1/4}Nb_{3/4})_xTiO_4$ ($x = 0.1$) ceramic of this study. In the Raman spectrum of the $Zr_{1-x}(Li_{1/4}Nb_{3/4})_xTiO_4$ ($x = 0.1$) ceramic, 16 scattering bands, centered at 131, 165, 196, 247, 284, 336, 379, 400, 430, 476, 538, 625, 653, 730, 815, and 868 cm^{-1} have been observed. Compared with those of the $Zr_5Ti_7O_{24}$ and $ZrTiO_4$ ceramic cooled at 1 °C/h, and the air-quenched $ZrTiO_4$ reported by other researchers,[17,18] as shown in Table I, most of the Raman bands of the $Zr_{1-x}(Li_{1/4}Nb_{3/4})_xTiO_4$ ($x = 0.1$) ceramic were related

Table I. Locations of the Raman bands of the $Zr_5Ti_7O_{24}$ and $ZrTiO_4$ ceramic cooled at 1 °C/h, air-quenched $ZrTiO_4$, and $Zr_{1-x}(Li_{1/4}Nb_{3/4})_xTiO_4$ ($x = 0.1$) ceramic.

Band	$Zr_5Ti_7O_{24}$[17]	$ZrTiO_4$ ceramic cooled at 1 °C/h[17]	Air-quenched $ZrTiO_4$[18]	$Zr_{1-x}(Li_{1/4}Nb_{3/4})_xTiO_4$ ceramic ($x = 0.1$)
1	—	—	124	131
2	210	—	158	165
3	215	—	—	196
4	245	248	258	247
5	282	290	269	284
6	310	—	—	—
7	340	331	331	336
8	380	377	394	379
9	400	409	415	400
10	430	421	—	430
11	450	444	—	—
12	475	479	—	476
13	535	538	537	538
14	625	612	590	625
15	650	650	625	653
16	730	724	646	730
17	800	810	795	815
18	—	—	—	868

to the 5 : 7 ordering phase. This indicates that the substitution of $(Li_{1/4}Nb_{3/4})$ for Zr in the $Zr_{1-x}(Li_{1/4}Nb_{3/4})_xTiO_4$ system enhanced the kinetics of the ordering reactions to form the $Z^{TT}Z_{TT}$ sequence (crystallized as the $Zr_5Ti_7O_{24}$ phase) instead of forming the low-T ordered $ZrTiO_4$ or the

high-T disordered $ZrTiO_4$ phase, which agreed well with the results of XRD analysis. Furthermore, an extra Raman band centered at about 868 cm^{-1} appeared and its relative intensity increased with substitution content. The relative intensities of 653/625 cm^{-1} changed markedly with the substitution content. Some weak Raman bands, such as those centered at 284, 538, and 730 cm^{-1} disappeared with increasing content of $(Li_{1/4}Nb_{3/4})$ substitution for Zr. On the other hand, the Raman bands centered at 625 and 336 cm^{-1} shifted to lower frequencies while those centered at 247 and 868 cm^{-1} shifted to higher frequencies.

For a dielectric in which more than one type of cations distribute randomly over the crystallographically equivalent sites, the broadening of Raman band and the shift of mode frequency are generally attributed to the following:[20,21] i) the anharmonic decay of optical phonons and ii) the scattering caused by compositional fluctuations. In the $Zr_{1-x}(Li_{1/4}Nb_{3/4})_xTiO_4$ system, there are two factors affecting the Raman vibrations of the samples. One is the $(Li_{1/4}Nb_{3/4})$ substitution; the other is the ratio of Zr/Ti, because the substitution changes this ratio, which would affect the occupation of the A and B sites by Zr and Ti. In the $Zr_5Ti_7O_{24}$ phase, the A sites [symmetry 4c (2)] were occupied by 0.968 Zr and 0.032 Ti ions and the B sites [symmetry 8d (1)] were occupied by 0.889 Ti and 0.111 Zr ions. With the content of Zr decreasing and/or Ti increasing, there would be more Ti ions occupying the Zr sites (such as A sites), which would affect the characteristics of the A and B sites in the $Zr_5Ti_7O_{24}$ phase and affect the vibrational spectroscopy accordingly. Our previous work[22] also shows that the relative intensity of the Raman peaks located at 653/625 cm^{-1} changes distinctly with the increasing Zr/Ti ratio. These two peaks were assigned to the vibration modes of the Zr–O and Ti–O octahedrons, respectively. Compared with the Raman spectrum of $Zr_5Ti_7O_{24}$,[17] the appearance of the Raman band centered at 868 cm^{-1} was correlated with the occupations of Li and Nb. Usually, the appearance of a new Raman mode reflects long-range or short-range cation ordering.[6,23] In complex perovskites, short-range cation ordering is apt to occur when the B sites are occupied by two or more types of cations with different electrovalences.[23] In this work, the short-range cation ordering of Li and Nb may have occurred, which was responsible for the appearance of the Raman band centered at 868 cm^{-1} in the $Zr_{1-x}(Li_{1/4}Nb_{3/4})_xTiO_4$ ceramics.

The Microwave dielectric properties of the $Zr_{1-x}(Li_{1/4}Nb_{3/4})_xTiO_4$ $(0.3 \le x \le 0.5)$ ceramics are shown in Fig. 5. The dielectric constant (ε_r) of the $Zr_{1-x}(Li_{1/4}Nb_{3/4})_xTiO_4$ $(x = 0.3)$ ceramic reached its maximum at 1140 °C and those of the $Zr_{1-x}(Li_{1/4}Nb_{3/4})_xTiO_4$ $(x = 0.4, 0.5)$ ceramics were stable with sintering temperature. As shown in Fig. 5(a), the dielectric constant of the $Zr_{1-x}(Li_{1/4}Nb_{3/4})_xTiO_4$ ceramic increased from 34.5 to 46.6 with increasing substitution content of $(Li_{1/4}Nb_{3/4})$ for Zr. The ionic polarizability of $(Li_{1/4}Nb_{3/4})^{4+}$ (3.28 $Å^3$) is slightly higher than that of Zr^{4+} (3.25 $Å^3$),[24] which was partially responsible for the increase in dielectric constant. The quality factor (Qf value) of the $Zr_{1-x}(Li_{1/4}Nb_{3/4})_xTiO_4$ ceramics increased from 20000 to 38000 GHz as the x value increased from 0.3 to 0.4 and then decreased to 30000 GHz as the x value increased further. The temperature coefficients of

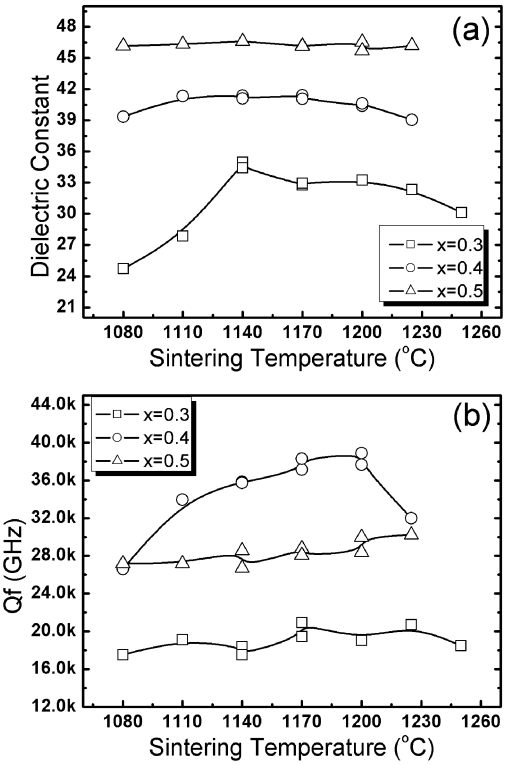

Fig. 5. Microwave dielectric properties [(a) dielectric constant and (b) Qf value] of $Zr_{1-x}(Li_{1/4}Nb_{3/4})_xTiO_4$ ceramics as a function of sintering temperature.

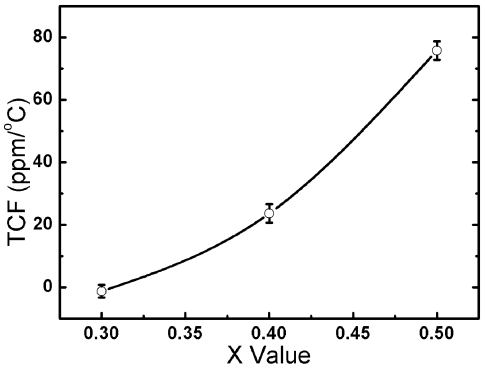

Fig. 6. TCF of $Zr_{1-x}(Li_{1/4}Nb_{3/4})_xTiO_4$ ceramics as a function of x value.

resonant frequencies (TCF) of the $Zr_{1-x}(Li_{1/4}Nb_{3/4})_xTiO_4$ ceramics as a function of the content of $(Li_{1/4}Nb_{3/4})$ substitution for Zr are presented in Fig. 6. The TCF value shifted from −1.2 to 75.8 ppm/°C when the x value increased from 0.3 to 0.5.

In general, the microwave dielectric properties depend greatly on many factors, such as grain size, porosity, grain boundary phase, chemical inhomogeneity, and domain size.[25] In the $Zr_{1-x}(Li_{1/4}Nb_{3/4})_xTiO_4$ system, $(Li_{1/4}Nb_{3/4})$ substitution improved the densification behavior of the ceramics and the dielectric loss decreased with increasing substitution content. On the other hand, the great distortion of the structure would increase the dielectric loss. Thus, the Qf value of the $Zr_{1-x}(Li_{1/4}Nb_{3/4})_xTiO_4$ ceramics showed maximum value when $x = 0.4$. Moreover, the $Zr_{0.6}(Li_{1/4}Nb_{3/4})_{0.4}TiO_4$ $(x = 0.4)$ ceramic showed a good micro-

structure with few pores and with uniform-size grains, as shown in Fig. 2, which was also partially responsible for the result that the $Zr_{0.6}(Li_{1/4}Nb_{3/4})_{0.4}TiO_4$ ($x = 0.4$) ceramic showed a maximum Qf value in the $Zr_{1-x}(Li_{1/4}Nb_{3/4})_xTiO_4$ system.

The ratio of Zr/Ti influenced the dielectric constant and the TCF value of the $Zr_{1-x}(Li_{1/4}Nb_{3/4})_xTiO_4$ ceramics greatly. As reported by Wang *et al.*,[16] the dielectric constant increased slightly with TiO_2 content for the air-quenched samples of the $ZrTi_{1+x}O_{4+x/2}$ ($0 \leq x \leq 0.3$) ceramics although the ionic polarizability of Ti^{4+} (2.93 Å^3) is smaller than that of Zr^{4+} (3.25 Å^3).[24] The $Zr_5Ti_7O_{24}$ phase and the $ZrTiO_4$ phase are two types of solid solution phases in the ZrO_2–TiO_2 system. In the $Zr_5Ti_7O_{24}$ phase, there will be more Ti ions occupying the octahedral center with the ratio of Ti/Zr increasing. The polarization of the Ti–O octahedron was higher than that of Zr–O octahedron, although the ionic polarizability of Ti^{4+} (2.93 Å^3) was smaller than that of Zr^{4+} (3.25 Å^3) because of its special structural character.[26] Then, the dielectric constant increased with the ratio of Ti/Zr. The TCF value was also related to the ratio of Zr/Ti in the $Zr_{1-x}(Li_{1/4}Nb_{3/4})_xTiO_4$ system. Our previous work[22] showed that the TCF value was likely to be negative when the ratio of Zr/Ti was close to 5 : 7 in the ZrO_2–$(Li_{1/4}Nb_{3/4})O_2$–TiO_2 system. For the $Zr_{1-x}(Li_{1/4}Nb_{3/4})_x$-$TiO_4$ ceramics, the ratio of Zr/Ti was much closer to 5 : 7 when $x = 0.3$, and the $Zr_{1-x}(Li_{1/4}Nb_{3/4})_xTiO_4$ ($x = 0.3$) ceramic showed a TCF value of -1.2 ppm/°C, which was near zero.

4. Conclusions

The phase evolution, sintering behavior, Raman vibration, and microwave dielectric properties of the $Zr_{1-x}(Li_{1/4}$-$Nb_{3/4})_xTiO_4$ system were investigated. XRD, BEI, and Raman spectroscopy analyse showed that all the Zr_{1-x}-$(Li_{1/4}Nb_{3/4})_xTiO_4$ ($0.1 \leq x \leq 0.5$) ceramics crystallized in the $Zr_5Ti_7O_{24}$ phase structure. Raman analysis showed that the substitution of $(Li_{1/4}Nb_{3/4})$ for Zr in the $Zr_{1-x}(Li_{1/4}$-$Nb_{3/4})_xTiO_4$ system enhanced the kinetics of the ordering reactions to form the $Z^{TT}Z_{TT}$ sequence. The abnormal Raman band centered at about 868 cm^{-1} in the Zr_{1-x}-$(Li_{1/4}Nb_{3/4})_xTiO_4$ ceramics may indicate the short-range cation ordering of Li/Nb. Without sintering aids, the sintering temperature of the $Zr_{1-x}(Li_{1/4}Nb_{3/4})_xTiO_4$ ceramic was lowered to 1110–1200 °C, which is much lower than that of $ZrTiO_4$ (higher than 1400 °C). The dielectric constant (ε_r) of the $Zr_{1-x}(Li_{1/4}Nb_{3/4})_xTiO_4$ ceramic increased from 34.5 to 46.6 and the temperature coefficient of resonant frequency (TCF) shifted from -1.2 to $+75$ ppm/°C as the content of $(Li_{1/4}Nb_{3/4})$ substitution increased from 0.3 to 0.5. The ratio of Zr/Ti influenced the dielectric constant and the TCF value of the $Zr_{1-x}(Li_{1/4}Nb_{3/4})_xTiO_4$ ceramics greatly.

Acknowledgements

This work was supported by the National 973 Project of China (2009CB623302), NSFC project of China (60871044), and Ph. D. Program Fund from the Ministry of Education of China (20060698007).

1) G. Wolfram and E. Göbel: Mater. Res. Bull. **16** (1981) 1455.
2) R. Christoffersen and P. K. Davies: J. Am. Ceram. Soc. **75** (1992) 563.
3) Y. Park, Y. H. Kim, and H. G. Kim: Mater. Sci. Eng. B **40** (1996) 37.
4) A. E. McHale and R. S. Roth: J. Am. Ceram. Soc. **66** (1983) C18.
5) A. E. McHale and R. S. Roth: J. Am. Ceram. Soc. **69** (1986) 827.
6) Y. K. Kim and H. M. Jang: J. Appl. Phys. **89** (2001) 6349.
7) V. Ličina, A. Gajović, A. Moguš-Milanković, I. Djerdj, N. Tomašić, and D. Su: J. Am. Ceram. Soc. **91** (2008) 178.
8) M. Dondi, F. Matteucci, and G. Cruciani: J. Solid State Chem. **179** (2006) 233.
9) H. Ikawa, A. Iwai, K. Hiruta, H. Shimojima, K. Urabe, and S. Udagawa: J. Am. Ceram. Soc. **71** (1988) 120.
10) Y. Higuchi and H. Katsube: US Patent 4665041 (1987).
11) Y. Park, N. H. Cho, and Y. H. Kim: US Patent 5432134 (1995).
12) Y. Park, N. H. Cho, and Y. H. Kim: US Patent 370580 (1994).
13) R. D. Shannon: Acta Crystallogr. **32** (1976) 751.
14) L. X. Pang, H. Wang, D. Zhou, and X. Yao: J. Am. Ceram. Soc. **91** (2008) 2947.
15) M. Valant, D. Suvorov, and R. C. Pullar: J. Eur. Ceram. Soc. **26** (2006) 2777.
16) C. L. Wang, H. Y. Lee, F. Azough, and R. Freer: J. Mater. Sci. **32** (1997) 1693.
17) F. Azough, R. Freer, and J. Petzelt: J. Mater. Sci. **28** (1993) 2273.
18) M. A. Krebs and R. A. Condrate, Sr.: J. Mater. Sci. Lett. **7** (1988) 1327.
19) P. Bordet, A. Mchale, A. Santoro, and R. S. Roth: J. Solid State Chem. **64** (1986) 30.
20) H. D. Fuchs, C. H. Greinm, C. Thomsen, M. Cardona, W. L. Hansen, E. E. Haller, and K. Itoh: Phys. Rev. B **43** (1991) 4835.
21) C. Ramkumar, K. P. Jain, and S. C. Abbi: Phys. Rev. B **53** (1996) 13672.
22) L. X. Pang, H. Wang, D. Zhou, and X. Yao: submitted to J. Phys. D.
23) H. Zheng, H. Bagshaw, G. D. C. Csete de Györgyfalva, and I. M. Reaney: J. Appl. Phys. **94** (2003) 2948.
24) R. D. Shannon: J. Appl. Phys. **73** (1993) 348.
25) K. Fukuda, R. Kitoh, and I. Awai: Jpn. J. Appl. Phys. **32** (1993) 4584.
26) L. Y. Zhang and X. Yao: *Physics of Dielectrics* (Xi'an Jiaotong University Press, Xi'an, 1979) p. 121.